LAWRENCE
LIVERMORE
NATIONAL
LABORATORY

Using Historic Models of Cn2 to predict r0 and regimes affected by atmospheric turbulence for horizontal, slant and topological paths

J. K. Lawson, C. J. Carrano

June 30, 2006

Disclaimer

Using Historic Models of C_n^2 to predict r_0 and regimes affected by atmospheric turbulence for horizontal, slant and topological paths

Janice K. Lawson[a] and Carmen J. Carrano[b]
Lawrence Livermore National Laboratory
Livermore, CA 94550

ABSTRACT

Image data collected near the ground, in the boundary layer, or from low altitude planes must contend with the detrimental effects of atmospheric turbulence on the image quality. So it is useful to predict operating regimes (wavelength, height of target, height of detector, total path distance, day vs. night viewing, etc.) where atmospheric turbulence is expected to play a significant role in image degradation. In these regimes, image enhancement techniques such as speckle processing, deconvolution and Wiener filtering methods can be utilized to recover near instrument-limited resolution in degraded images. We conducted a literature survey of various boundary layer and lower troposphere models for the structure coefficient of the index of refraction (C_n^2). Using these models, we constructed a spreadsheet tool to estimate the Fried parameter (r_0) for different scenarios, including slant and horizontal path trajectories. We also created a tool for scenarios where the height along the path crudely accounted for the topology of the path. This would be of particular interest in mountain-based viewing platforms surveying ground targets. The tools that we developed utilized Visual Basic® programming in an Excel® spreadsheet environment for accessibility and ease of use. In this paper, we will discuss the C_n^2 profile models used, describe the tools developed and compare the results obtained for the Fried parameter with those estimated from experimental data.

Keywords: Atmospheric turbulence, atmospheric boundary layer, index of refraction, structure coefficient, C_n^2, Fried parameter

1. ATMOSPHERIC BOUNDARY LAYER

In this treatment, we are assuming day conditions and an atmosphere that can be described by conventional atmospheric boundary layer models. The difficulty associated with the second assumption is clear from the definition provided by the American Meteorological Society Glossary of Meteorology for the atmospheric boundary layer:

> (Abbreviated ABL; also called boundary layer, planetary boundary layer) The bottom layer of the troposphere that is in contact with the surface of the earth. It is often turbulent and is capped by a statically stable layer of air or temperature inversion. The ABL depth (i.e., the inversion height) is variable in time and space, ranging from tens of meters in strongly statically stable situations, to several kilometers in convective conditions over deserts…During daytime, a mixed layer of vigorous turbulence grows in depth, capped by a statically stable entrainment zone of intermittent turbulence...[1]

This region of the troposphere is largely unstable and challenging to characterize in even a temporally averaged sense. Properties are strongly influenced by surface morphology and local temperature gradients. Nevertheless, the surface layer is often the location of a remote sensing platform (whether ground-based or low altitude aerial) and the atmospheric turbulence associated with the ground layer will often dictate the quality of the imaging.

We use the Fried parameter (r_0) as a metric for characterizing the strength of the atmospheric turbulence. By integrating the magnitude of $C_n^2(z)$ over a weighted path integral, Fried developed an expression for a turbulence coherence length, r_0, which defines an effective aperture over which the mean-squared wavefront remains coherent (i.e. is less than 1 rad^2) after propagating through the atmosphere[2]. Hence, imaging properties in poor seeing conditions are not always dictated by the aperture of the imaging system, but can instead be determined by the diffraction limit imposed by this potentially smaller coherence length. For the spherical wave approximation applicable for most remote imaging application, the Fried parameter[3] is calculated as:

$$r_0 = 0.185 \left[\frac{4\pi^2}{k^2 \int_0^L dz \left(\frac{L-z}{L}\right)^{5/3} C_n^2(z)} \right]^{3/5}, \tag{1}$$

where the integration is from the pupil plane at $z = 0$ over the path length to $z = L$. Note that $k = 2\pi/\lambda$ where λ is the wavelength being imaged.

2. HISTORICAL MODELS USED (WITH CAVEATS)

Models of C_n^2 exist at many levels of complexity[4]. We chose to incorporate historical models of C_n^2 based mainly on their common use in literature, the availability of the algorithm in open literature and/or their ease in programming into simple routines. It was beyond the scope of this work to incorporate satellite data from weather stations in order to predict current atmospheric conditions. Rather, we wished to study reasonable trending to parametric variations of target vs. observation height for various remote sensing scenarios. Of particular interest to us were differences in visible, NIR and MWIR ground-based or low altitude observations over horizontal path, slant path and more complex topologies.

We also note that although Equation 1 utilizes the symbol $C_n^2(z)$, the profile models developed explicitly express C_n^2 as a function of height above the ground, i.e. $C_n^2(h)$. Models incorporated into our study include a general height^(-4/3) model based on early similarity theory and observations, the well-known Hufnagel-Valley model, a Kaimal model developed by Walters and Kunkel, a modified Kukharets and Tsvang model, a model developed by Brookner, the Satellite Laser Communications – Day (SLC-D) model, and a model developed by Ryznar and Bartlo. Each of these models attempts to model the dependence of a temporal average value of atmospheric turbulence as a function of height. However, none of the models can properly treat the ground layer, an inherent weakness in the approach we are taking. Each model requires special attention to its strengths and weaknesses. Note: C_n^2 units in this report are m$^{-2/3}$.

2.1 Kaimal-type models

The simplest model of C_n^2 is based on similarity theory descriptions of the boundary-layer turbulence[5] in order to predict the dependence of C_n^2 with height. The daytime exponential altitude falloff is modeled as $-4/3$ power and the range of validity extends to approximately one-half the height of the boundary-layer inversion. Walters and Kunkel[6] further refined the power law model to include details of the behavior approaching the inversion layer developed by Kaimal et al.[5] for C_T^2. This expanded the model to the following form:

$$\frac{C_n^2(h)}{C_n^2(h_0)} = \begin{cases} \left(h/h_0\right)^{-4/3} & h_0, h \le 0.5h_i \\ \left(0.5h_i/h_0\right)^{-4/3} & 0.5h_i \le h \le 0.7h_i \\ 2.9\left(0.5h_i/h_0\right)^{-4/3}\left(h/h_i\right)^3 & 0.7h_i \le h \le h_i \end{cases}, \tag{2}$$

where h_i is the height of the inversion layer above ground and h_0 is a reference altitude (often taken to be a tower level) and assumed to be above the surface layer. The region of validity for this model extends to the height of the inversion layer.

Kukharets and Tsvang[7] developed the Kaimal-type profile model further by adding an exponential fall-off for C_n^2 above the inversion layer. Murphy, Dewan and Sheldon[8] clarified this result and generalized the model to allow the use of any reference height measurement of C_n^2 near the surface. This resulted in a "modified" Kukharets/Tsvang model of the form:

$$\frac{C_n^2(h)}{C_n^2(h_0)} = \frac{k_1\left(\dfrac{h}{h_i}\right)^{-4/3} + k_2 e^{-k_3\left(\frac{h}{h_i}-1.1\right)^2}}{k_1\left(\dfrac{h_0}{h_i}\right)^{-4/3}},$$

(3)

where h_0 is a reference height, h_i is the height of the inversion layer, $k_1 = 4.6 \times 10^{-2}$, $k_2 = 0.6$ and $k_3 = 12$. Although this model extends down to near the surface, implicit in the derivation is the assumption that the thin surface-layer turbulence is omitted. The model assumed heights at or above some observing station.

2.2 Parametric fits to experimental data

Another popular model for the altitude scaling of C_n^2 was developed by Hufnagel[9] and augmented with a boundary layer term extending the model to the surface, as suggested by Valley[10]. In contrast to the theoretical basis of the Kaimal-type models, the Hufnagel-Valley model is an empirical fit to observed dependences of $C_n^2(h)$ in a mid-latitude climate. It is a parametric model with two variables; A, which represents relative strength of the turbulence near the ground level and v, which represents high altitude wind speed. The Hufnagel-Valley model is given by:

$$C_n^2(h) = 5.94 \times 10^{-53}(v/27)^2 h^{10} e^{(-h/1000)} + 2.7 \times 10^{-16} e^{(-h/1500)} + A e^{(-h/100)},$$

(4)

where commonly used values of the parameters are $A = 1.7 \times 10^{-14}$ m$^{-2/3}$ and v = 21 m/s, although v = 57 m/s is sometimes used for stronger wind conditions.

Similarly, Brookner[11] proposed a numerical model based on Hufnagel's experimental data. It has the form:

$$C_n^2(h) = C_{n0}^2 h^{-b} e^{(-h/h_0)} + C_{np}^+ \delta(h - h_p),$$

(5)

where $\delta(h)$ is the delta function and C_{np}^+ represents the integral of $C_n^2(h)$ under its peak which occurs at the tropopause altitude of $h = h_p = 12$km. Values of the parameters suggested for sunny day conditions are $b = 5/6$, $h_0 = 320$ m and $C_{n0}^2 = 3.6 \times 10^{-13}$. Alternate parameters are suggested for clear night and dawn-dusk conditions.

2.3 SLC-D model

One of the commonly used models with no parameters is the Submarine Laser Communications-Day (SLC-D) model[12]. This C_n^2 profile model is based on data collected from the AMOS telescope site at the top of Mt. Haleakala, Hawaii. Care needs to be taken in using this model because of the unique topology of the site and the subtropical climate. Nonetheless, it is an easy model to include for comparison. The model has the following form:

$$C_n^2(h) = \begin{cases} 1.70 \times 10^{-14} & h < 18.5m \\ 3.13 \times 10^{-13}/h & 18.5m < h < 240m \\ 1.30 \times 10^{-15} & 240m < h < 880m \\ 8.87 \times 10^{-7}/h^3 & 880m < h < 7,200m \\ 2.00 \times 10^{-16}/h^{0.5} & 7,200m < h < 20,000m \end{cases}.$$

(6)

A similar model is available for nighttime conditions. An alternate version of the SLC-D profile model is listed in publications[13,14] as:

$$C_n^2(h) = \begin{cases} 0 & 0m < h < 19m \\ 4.008 \times 10^{-13} h^{-1.054} & 19m < h < 230m \\ 1.300 \times 10^{-15} & 230m < h < 850m \\ 6.352 \times 10^{-7} h^{-2.966} & 850m < h < 7,000m \\ 6.209 \times 10^{-16} h^{-0.6229} & 7,000m < h < 20,000m \end{cases}, \tag{7}$$

which has a disturbing treatment of the ground layer. Figure 1 shows a comparison of the behaviors of the two versions of the profile model. While the high altitude behavior is very similar, the ground layer behavior of C_n^2 is absent in the second version of the profile model. This makes the second version unsuitable for modeling of ground-based observations.
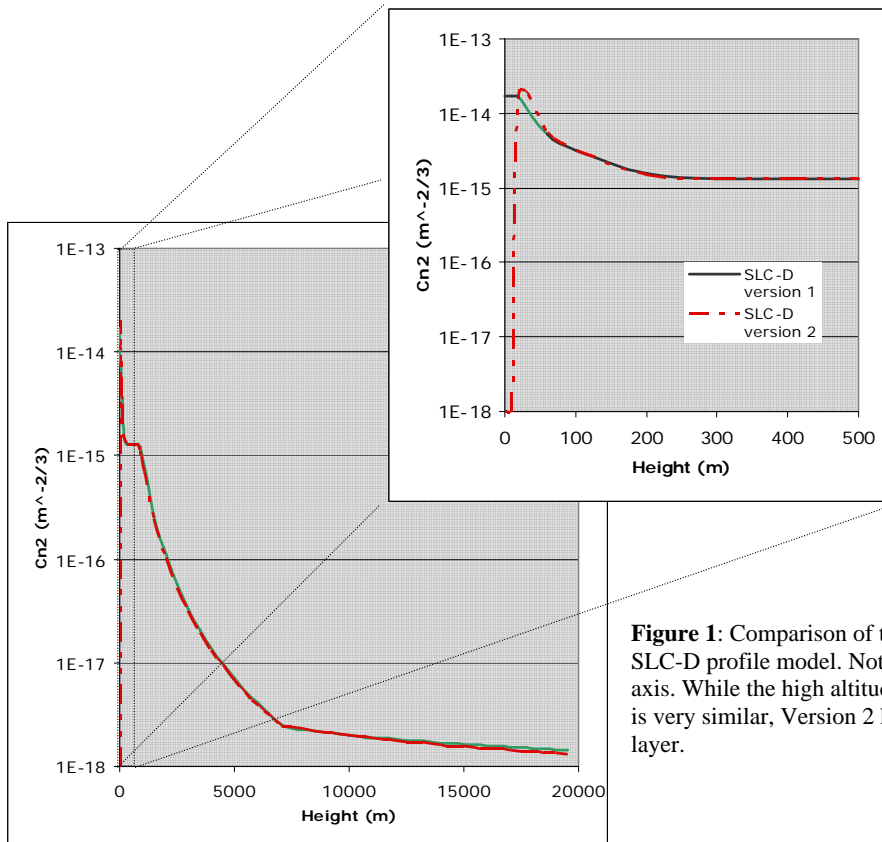

Figure 1: Comparison of two published versions of the SLC-D profile model. Note the logarithmic scale on the y axis. While the high altitude behavior of the two versions is very similar, Version 2 has no treatment of the ground layer.

2.4 Heat flux model

The final profile model included in the current study is one that estimates the heat flux from the ground based on the latitude and longitude, as well as the date, time and cloud cover[15]. Published by Ryznar and Bartlo, the profile model takes nine input parameters to estimate $C_n^2(h)$. We experienced some difficulty with the published algorithm and resorted to using only the parameters published in the report. These parameters modeled a desert location in White Sands, NM midday in early September.
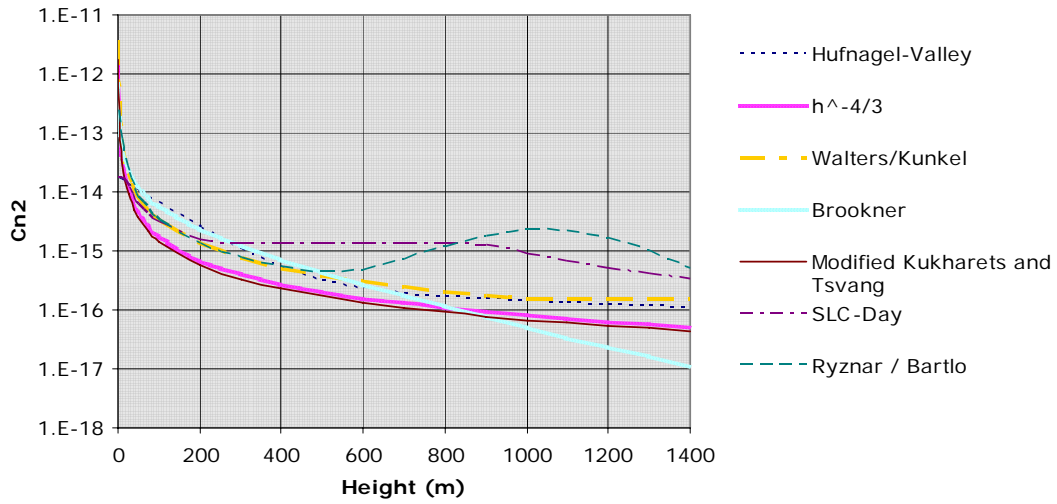
Figure 2: Surface layer behavior of the various profile models discussed using parameters listed in references.

2.4 Model comparisons

Figure 2 depicts the surface layer behavior of the various profile models described above. For those models requiring input parameters, we use those listed in the original reports. The general behavior of all the models is similar, with the ground layer treatment being the most notable difference between the models. However, two models (SLC-D and Ryznar/Bartlo) also show higher estimate of C_n^2 above about 600m than the other models.

These profile models represent a sampling of the different type of models available. This does not begin to constitute a complete set, but provides a basis set to investigate variations of r_0 with distance, wavelength and topology for scenarios of interest.

3. WORKSHEET DEVELOPMENT

Each of the described profile models was programmed in Visual Basic[©] embedded in an Excel[©] workbook. Within the workbook, we provided easy access for variation in parameters for those profile models requiring input, while noting the values of the parameters included in the originating reports. In the Visual Basic[®] routines, we also included an algorithm for Romberg integration,[16] which allowed ready numerical evaluation of integral equations. We then chose to represent various remote sensing scenarios: a) air-borne slant path from relatively low altitude (aerostat, UAV or manned plane), b) ground-based horizontal path and c) elevated ground-based platform with options in topology over the path. These options were straightforward to implement by taking the integral expressed in Equation (1) over the path z while noting that $h(z)$ and $C_n^2(h)$. The options only required different representations for $h(z)$. Figure 3 illustrates a parametric model of $h(z)$ consisting of a triangular mountain of variable height and width, a variable height valley and a variable height and width plateau on which the target is located.

A similar routine was also developed for calculating the anisoplanatic angle, θ_0, given by[17]

$$\theta_0 = \left\{ 2.905k^2 \int_{PATH} dz C_n^2(z) z^{5/3} \right\}^{-3/5}, \tag{8}$$

giving us what Fried noted as "almost all the dependence on the distribution of the strength of turbulence in the dependence of r_0 and θ_0 on these quantities." The results from the anisoplanatic angle calculations will not be presented here, due to space constraints.
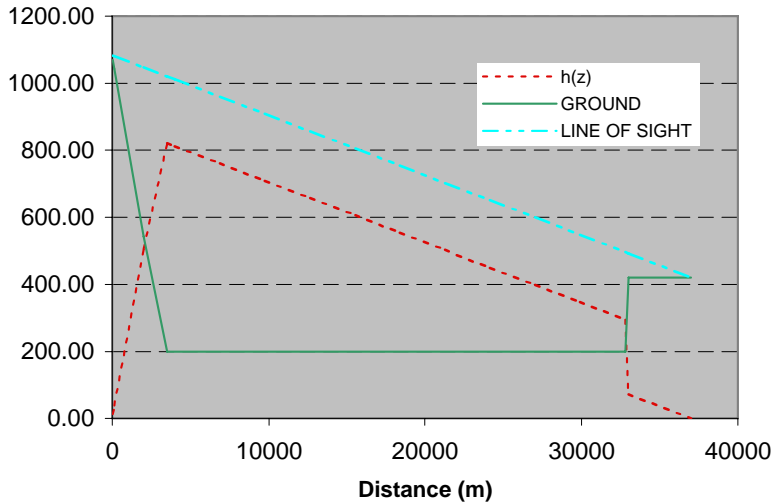

Figure 3: A topological model of $h(z)$ for a path from a mountain over a valley to a target on a plateau. Note: the heights of the mountain and valley correspond roughly to Mt. Diablo, CA and the neighboring Livermore Valley. In this example, the height and width of the plateau were chosen to mimic the location of targets shown in Figure 6. Airborne platforms can be modeled by setting the height of the plateau to the height of the valley and setting the width of the mountain to zero.

One complication occurred during implementing this process that warrants comment. The Romberg algorithm worked well for the task, but needed refinement when using the complex topology. The change in slope of $h(z)$ when transitioning from one region to another violated the assumption of a smoothly varying function and required the integral to be broken into two or more segments. An additional improvement in the accuracy of the calculations may be possible for non-smoothly varying models of $C_n^2(h)$ if the integrals are further broken into regions over which C_n^2 is required to be smoothly varying.

4. CALCULATIONS AND COMPARISON WITH DATA

In order to test whether the r_0 values produced by the calculations were reasonable, we compared the values to estimated r_0 values calculated with a spectral ratio technique[18]. Four scenarios previously described in the literature[19] (with improved speckle processed imagery shown here from the original published results) were used as the basis for the evaluation and are summarized in Figures 4-7. Distances and elevations were estimated using the assistance of Google Earth[©]. Parameters used for the comparison, as well as the results, are summarized in Tables 1 and 2.
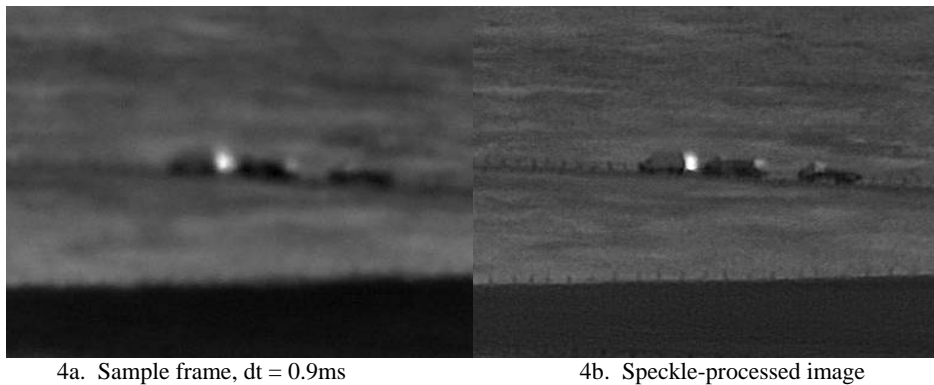

| 4a. Sample frame, dt = 0.9ms | 4b. Speckle-processed image |

Figure 4: Three trucks from 22 km range. All images (figures 4-7) are taken from Mt. Diablo (elevation 1083m). Elevation of targets is approximately 200m. The estimate for r_0 for this image is about 1 cm.

5a. Sample frame, dt = 2 ms   5b. Speckle-processed image

Figure 5: Three trucks from 29 km range. Targets located on valley floor (200m). The estimate for r_0 is about 1 cm.

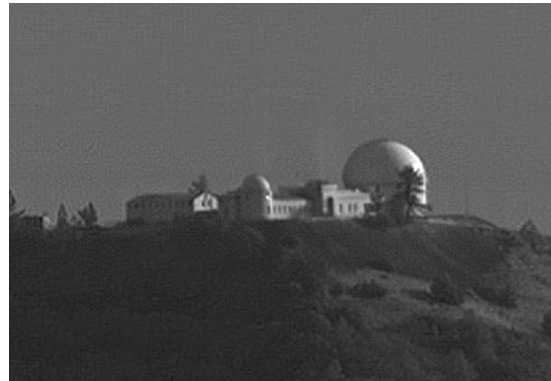

6a. Sample frame, dt = 1 ms   6b. Speckle-processed image

Figure 6: Same three trucks at 37 km range. Targets located at an elevation of about 420m. The location is on an elevated plateau extending approximately 4 km in front of the targets. The estimate for r_0 based on this image is about 1 cm.

7a. Sample frame, dt = 1 ms   7b. Speckle-processed image

Figure 7: Lick Observatory as seen from Mt. Diablo, 64 km range. The elevation of the observatory is approximately 1273m. There is little evidence of a plateau in the vicinity of Mt. Hamilton. The estimate for r_0 for this image is approximately 1.5 to 2 cm.

Model	Parameters used in references	"Tuned" Parameters
$h^{-4/3}$	n/a, we used $C_n^2(0.5m) = 2e-12$	No change
Walters & Kunkel	$C_n^2(9m) = 8.e-14$, $z_i=2000m$	$C_n^2(9m) = 4.e-14$, $z_i=2000m$
Mod. Kukharets & Tsvang	$C_n^2(14m) = 2.e-14$, $z_i=3000m$	No change
Hufnagel-Valley (HV-21)	A=1.7e-14, v=21 m/s	A=3e-14, v=21 m/s
Brookner	$C_n^2(320m) = 3.6e-13$, b=0.833	$C_n^2(320m) = 3e-13$, b=0.833
SLC-D	n/a	n/a
Ryznar & Bartlo	Date=840908, t=1344, cld cover(in tenths)=1, cld height code =5, wind speed = 0.9, h(mix layer) = 950m, lat = 32.4, long = 106.37, zone =105	n/a

Table 1: Parameters used for the various C_n^2 profile models. C_n^2 units are $m^{-2/3}$

r_0 (cm) Calculated based on Mountain-top Platform								
Target Location	Topology parameters	C_n^2 Profile Model						
		$h^{-4/3}$	Walters & Kunkel	Mod. Kukharets & Tsvang	HV-21	Brookner	SLC-D	Ryznar & Bartlo
Valley, z=22km	h_{mt} =1083m, h_{valley} =200m, w_{mt} = 4000m	1.451	0.992 *1.503*	1.600	1.968 *1.460*	1.408 *1.570*	1.625	1.419
Valley, z=29km	h_{mt} =1083m, h_{valley} =200m, w_{mt} = 4000m	1.457	0.995 *1.509*	1.606	1.885 *1.411*	1.384 *1.544*	1.433	1.352
Plateau, z=37km	h_{mt} =1083m, h_{valley} =200m, w_{mt} = 4000m, $h_{plateau}$ = 420m, $w_{plateau}$ = 4km	1.493	1.020 *1.546*	1.646	2.005 *1.608*	1.455 *1.623*	1.279	1.261
Mt top, z=65km	h_{mt} = 1083m, h_{valley} = 200m, w_{mt}= 4000m, $h_{plateau}$ = 1273m, $w_{plateau}$ = 500m	1.545	1.055 *1.600*	1.703	2.033 *1.528*	1.614 *1.801*	1.049	0.722

Table 2: Fried parameter calculated using various C_n^2 profile models with published parameters (plain text) and with "tuned" parameters (italics)

5. OBSERVATIONS

For the C_n^2 profile models based on similarity theory, the trends with varying scenarios follows the trends observed in the data. The models based on an experimental fit to the Hufnagel data showed similar trends. However, both the SLC-D and Ryznar/Bartlo models showed markedly different trends. We already know that the SLC-D model is based on a unique geographical location, so this difference may not be unexpected. The Rynar/Bartlo model also used a relatively low height for the mix layer in the parameters published in the report (i.e. 950m). Close inspection of the model comparison in Figure 2 can also help explain the behavior. Both the SLC-D and Ryznar/Bartlo models produce noticeably larger estimates of C_n^2 at heights of 600 – 1000m.

The similarity of the results for "untuned" models is encouraging. Also encouraging is rough order of magnitude agreement of the model with the data. Although none of the models produce the significant increase in r_0 seen in the last scenario, the increase in path length did not create a reduction in r_0 for any except the last two models.

Dropping the last two models for the moment, we can attempt to tune the remaining models to produce more similar profiles than resulted from the original reports. Table 1 lists the modified values of the

parameters. This particular choice of parameters makes the remaining models roughly overlay at a height of 15m. Figure 8 illustrates the difference in ground layer behavior between the models with this choice of parameters. The calculated values of r_0 with the modified parameters are listed in Table 2 in italics.
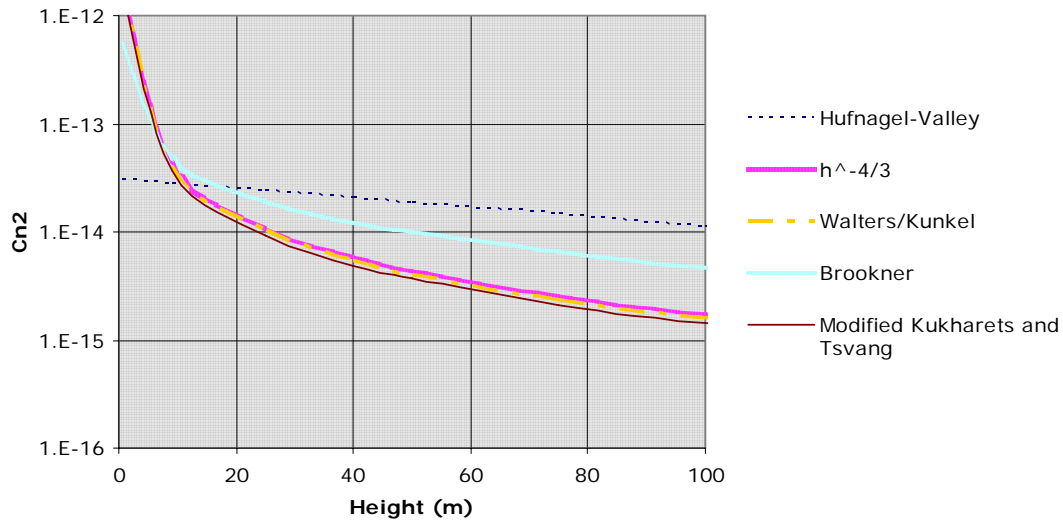

Figure 8: Surface layer behavior of the selected profile models discussed using modified parameters.

Analyzing the trends in the calculations produced by the modified parameters, it appears that the Brookner model might be showing the closest trend to that apparent in the data, suggesting that the ground layer near Mt. Diablo may not be following a -4/3 power law, but one slightly less. One other possible explanation for the apparent larger r0 than calculated may lie in details of the topology neglected in the simple model. The first three scenarios were obtained looking in much the same direction. The fourth scenario looked in a slightly different direction. Study of the topology in that direction suggests that the mountain is not as wide in that direction as in the direction sampled by the first three scenarios. The calculation of r_0 is very sensitive to the region near the platform, so neglecting details such as this may complicate detailed comparisons of data and calculations.

Although including details of the topology near the viewing platform is critical to the results, details of the topology near the target are not as critical (due to the (L-z)/L factor in the integrand). So including the option for a variable height and width plateau at the target did not significantly affect the results. Results in the next section are done with the simpler topology of a target located on the valley floor.

6. CONCLUSIONS

Using the "tuned" version of the selected C_n^2 profile models, we can now extrapolate behavior for different remote sensing conditions and wavelengths. For these studies, we show only the results of the Brookner model, although the other models produce very similar results. We used three wavelengths: visible (0.5 micron), short-wave infrared (SWIR) (1.2 micron) and mid-wave infrared (MWIR) (4 microns). The first case we describe is a variation on the mountain platform scenario. Keeping the height and width of the mountain constant and the target on the valley floor, we vary the distance to the target (Figure 9a). Then, we vary the seeing conditions, by doubling the $C_n^2(320m)$ (Figure 9b). Although much of the behavior seen here is expected (such as the improvement in r_0 with longer wavelength and the degradation with increasing C_n^2), the relative independence of r_0 with distance to the target is interesting. Also interesting is the "knee" in the curve at short distances. This happens when the target nears the base of the mountain and the path approximates a horizontal path as it follows the slope of the mountain. Not shown, but also demonstrated by the model, r_0 increases with a decrease in the width of the mountain or an increase in the height of the mountain for a fixed with.

Mountain Topology
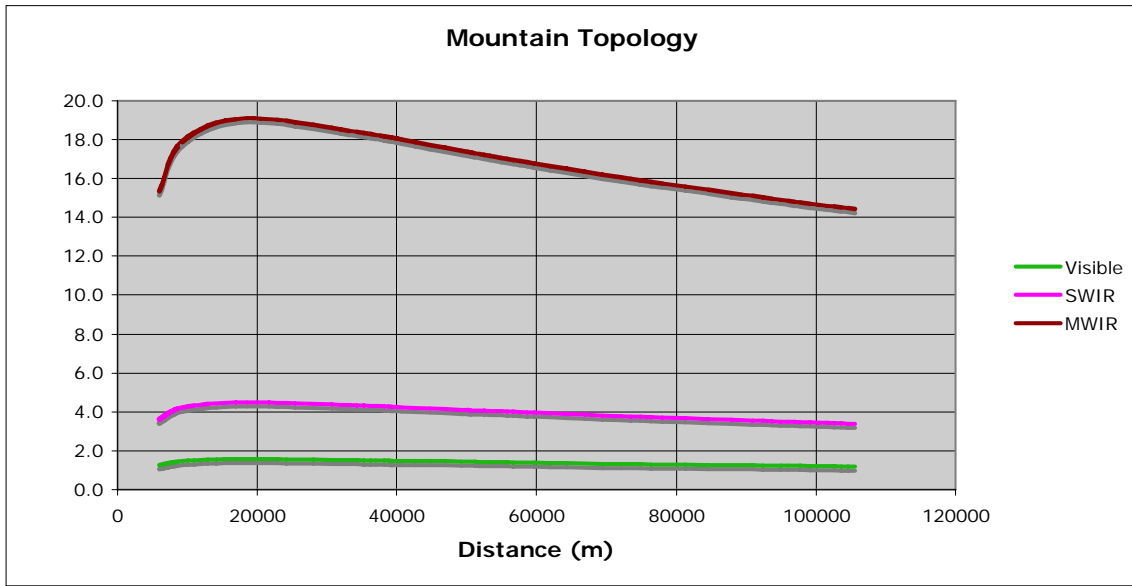
(a) Brookner model using "tuned" parameters

Mountain Topology
Doubling Cn2(0)
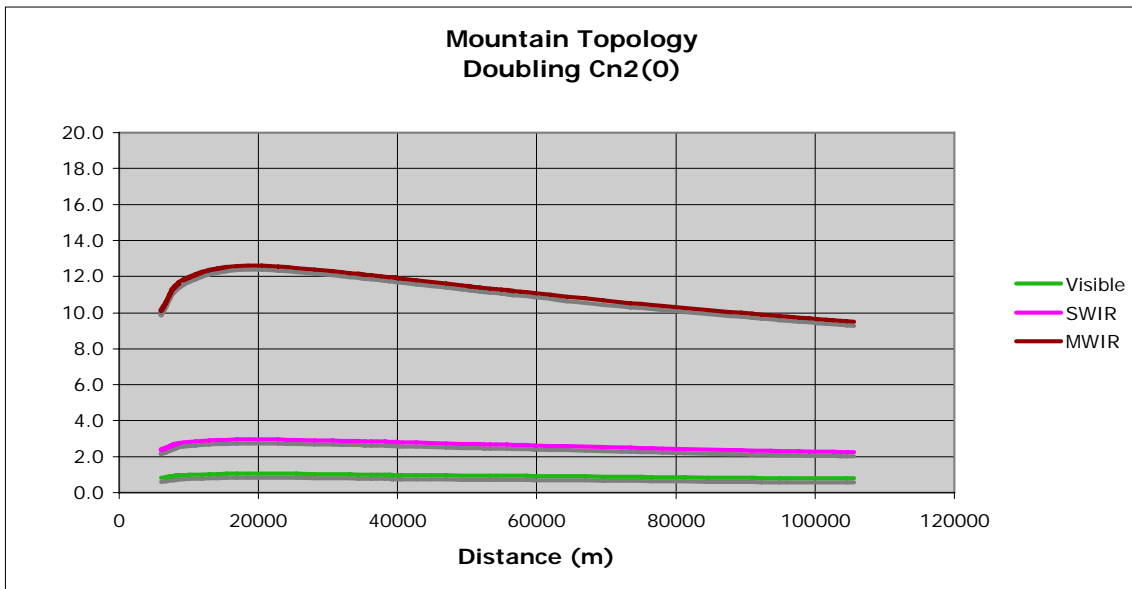
(b) Brookner model using $C_n^2(320m) = 6e\text{-}13$

Figure 9. Results for different wavelength remote imaging scenarios based on a mountain altitude of 1083m and width of 4000m. The target is assumed on a valley floor of altitude 200m.

By setting the width of the mountain to be vanishingly small, we use the same model to investigate a remote imaging scenario that uses an unmanned aerial vehicle (UAV), an aerostat or similar aerial platform. Figure 10 illustrates the results for each of the chosen wavelengths. The altitude of the aerial platform is held constant at 500m while the distance to the target is varied. This creates a family of slant paths. Without the topology of the mountain, r_0 steadily degrades for increasing distance to the target. Higher altitude platforms show increasing improvement in r_0 with height. For this result, the poor seeing condition was used yet values of r_0 remain quite good for all but the longer paths using visible wavelengths.
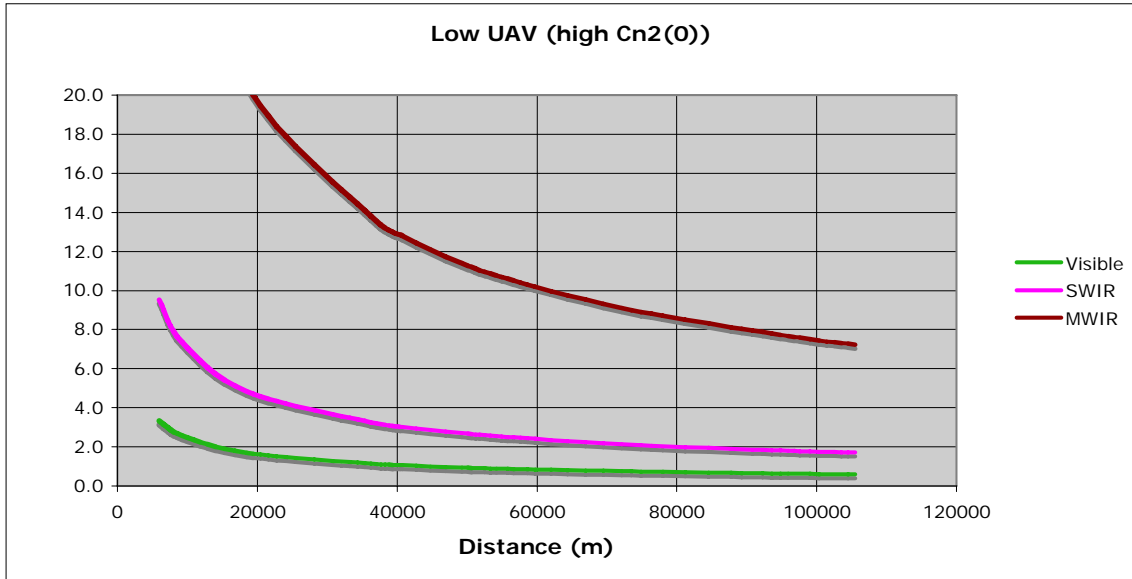
Figure 10. Results from Brookner model for an aerial platform 500m above ground using $C_n^2(320m) = 6e\text{-}13$.
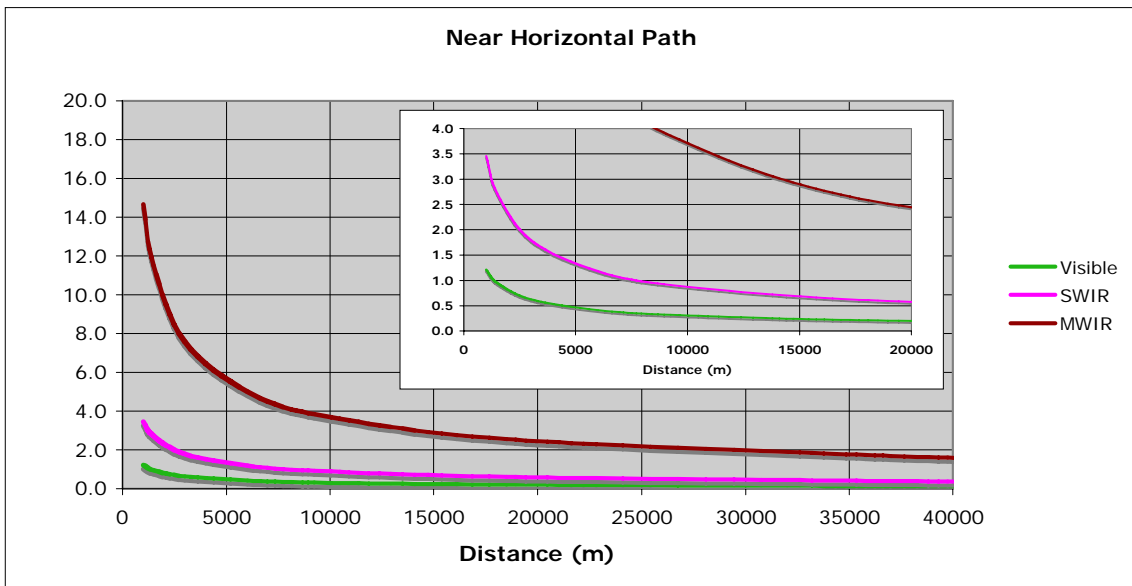

Figure 11. Results from Brookner model for a near horizontal path in nominal seeing conditions. Values near the origin are displayed in the inset.

The final scenario described here is the most challenging for remote imaging – horizontal or near-horizontal path. Figure 11 demonstrates that even the longer wavelengths suffer degradation in r_0 for the nominal seeing conditions represented by the "tuned" parameters. For this result, the platform was elevated 10 meters above ground and the target. Doubling the height platform increases r_0 by approximately 50%. Note that the scale on r_0 has been held constant on Figures 9 – 11. The distance range is also constant except on Figure 11 where it is shortened to 40 km.

These scenarios represent only a fraction of the ones of possible interest for remote imaging. The results demonstrate the importance of the platform location and the topology, especially near the platform. The spreadsheet developed is sufficiently flexible that better models of ground layer C_n^2 profiles can easily be incorporated.

ACKNOWLEDGEMENTS

REFERENCES

1. R.B. Stull, *An Introduction to Boundary Layer Meteorology*, pp. 666, Kluwer Academic Publishers, Dordrecht, The Netherlands,1988.
2. J.W. Hardy, *Adaptive Optics for Astronomical Telescopes*, p. 29 and p.92, Oxford University Press, NY,NY, 1998.
3. M.C. Roggemann, *Imaging Through Turbulence*, p.73, CRC Press, Boca Raton, FL, 1996.
4. A few of the useful summaries that exist include: (a) R.R. Beland, "Propagation through Atmospheric Optical Turbulence," in *The Infrared and Electro-optical Systems Handbook, Vol.2 – Atmospheric Propagation of Radiation*, pp. 212-232, SPIE Optical Engineering Press, Bellingham, WA, 1993, (b) Roggemann, Michael C., *Imaging Through Turbulence*, p61-67, CRC Press, Boca Raton, FL 1996, (c) R.E. Good, R.R. Beland, E.A. Murphy, J.H. Brown and E.M. Dewan, "Atmospheric Models of Optical Turbulence", SPIE, **928**, pp 165-186, 1988 or (d) Tunick,Arnold, "A Critical Assessment of Selected Past Research on Optical Turbulence Information in Diverse Microclimates", ARL-ML-521, Army Research Laboratory, Adelphi, MD, July 2002.
5. J.C. Kaimal, J.C. Wyngaard, D.A. Haugen, O.R.Cote and Y. Izumi, "Turbulence structure in the convective boundary layer", J. Atmos. Sci. **33**, pp. 2152-2169, 1976.
6. D.L. Walters and K.E. Kunkel, "Atmospheric modulation transfer function for desert and mountain locations: the atmospheric effects on r_0", J. Opt. Soc. Am., **71**(4), pp. 397-405, 1981.
7. V.P. Kukharets and L.R. Tsvang, "Structure Parameter of the Refractive Index in the Atmospheric Boundary Layer", Izvestiya, Atmospheric and Oceanic Physics, **16**(2), pp. 73-77,1980.
8. E.A. Murphy, E.M. Dewan, and S.M. Sheldon, "Daytime comparisons of C_n^2 models to measurements in a desert location", SPIE, **551**, pp. 156-162, 1985.
9. R.E. Hufnagel, "Propagation through atmospheric turbulence", in *The Infrared Handbook*, Chapter 6, USGPO, Washington,D.C., 1974.
10. G.C. Valley, "Isoplanatic degradation of tilt correction and short-term imaging systems," Appl. Opt. **19**, pp. 574-577, 1980.
11. E. Brookner, "Improved Model for the Structure Constant Variations with Altitude", Applied Optics, **10**(8), pp.1960-1962, 1971.
12. R.E. Good, R.R. Beland, E.A. Murphy, J.H. Brown and E.M. Dewan, "Atmospheric Models of Optical Turbulence", SPIE, **928**, pp 165-186.
13. R.R. Parenti and R.J. Sasiela, "Laser-guide-star systems for astronomical applications", J. Opt. Soc. Am. A, **11**(1), pp. 288-309, 1994.
14. M.C. Roggemann and B.M. Welsh, *Imaging Through Turbulence*, p.62, CRC Press, Boca Raton, FL, 1996.
15. E. Ryznar and J.A. Bartlo, "Dependence of Cn2(ci2) in the Atmospheric Boundary Layer on Conventional Meteorological Variables," AFGL-TR-86-0013 (ADA169478), Air Force Geophysics Laboratory, Hanscom Air Force Base, MA,1985.
16. W.H Press, S.A. Teukolsky, W.T. Vetterling, B.P. Flannery, *Numerical Recipes in Fortran 77*, Chapter 4, Cambridge Press, NY, NY, 1992.
17. D.L. Fried, "Anisoplanatism in adaptive optics", J. Opt. Soc. Am., **72**, pp 52-61, 1982.
18. O. von der Lühe, "Estimating Fried's parameter from a time series of an arbitrary resolved object imaged through atmospheric turbulence", J. Opt. Soc. Am. A, **1**(5),pp. 510-519, 1984.
19. C.J. Carrano," Progress in Horizontal and Slant-Path Imaging Using Speckle Imaging", SPIE, **5001**, pp. 56-64, 2003.